Biosensors and Bioelectronics 145 (2019) 111716

Contents lists available at ScienceDirect

Biosensors and Bioelectronics

journal homepage: www.elsevier.com/locate/bios

In-situ reduction of Ag^+ on black phosphorene and its NH_2-MWCNT nanohybrid with high stability and dispersibility as nanozyme sensor for three ATP metabolites

Ting Xue[a,b,1], Yingying Sheng[b,1], Jingkun Xu[a,d,*], Yingying Li[a,b], Xinyu Lu[a,b], Yifu Zhu[a,b], Xuemin Duan[a], Yangping Wen[b,c,**]

[a] School of Pharmacy, Jiangxi Science & Technology Normal University, Nanchang, 330013, China
[b] Institute of Functional Materials and Agricultural Applied Chemistry, Jiangxi Agricultural University, Nanchang, 330045, China
[c] Key Laboratory of Crop Physiology, Ecology and Genetic Breeding, Ministry of Education, Jiangxi Agricultural University, Nanchang, 330045, China
[d] College of Chemistry and Molecular Engineering, Qingdao University of Science & Technology, Qingdao, 266042, China

ARTICLE INFO

Keywords:
Black phosphorene
Nanozyme sensor
Voltammetric analysis
Environmental stability
Water-processibility

ABSTRACT

The environmental stability, water-processibility and life-span of black phosphorene (BP) severely limit the application of its electronic devices in aqueous system containing oxygen. We reported the controllable preparation of in-situ reduction and deposition of silver nanoparticles on the BP surface and its amino-functionalized multi-walled carbon nanotubes (NH_2-MWCNT) nanocomposite. With the addition of both NH_2-MWCNT and Ag^+, the BP-based nanocomposite was prepared by ultrasonic-assisted liquid-phase exfoliation and was dispersed in carboxymethyl cellulose sodium (CMC) aqueous solution. The morphology, microstructure, and electrochemical properties of the nanohybrid were characterized. NH_2-MWCNT-BP-AgNPs showed high environmental stability, good water-processibility, satisfactory life-spans, superior electrocatalytic capacity with enzyme-like kinetic characteristics. The nanohybrid was applied as electrochemical sensors for single/simultaneous analysis of uric acid (UA), xanthine (XT) and hypoxanthine (HX). Excellent voltammetric responses for simultaneous determination in linear ranges of 0.1–800 μM with a limit of detection (LOD) of 0.052 μM for UA, 0.5–680 μM with a LOD of 0.021 μM for XT, and 0.7–320 μM with a LOD of 0.025 μM for HX under optimal conditions. Besides, the developed nanozyme sensor was employed for simultaneous voltammetric analysis of UA, XT and HX in real samples with acceptable recoveries. This work will provide theoretical guidance and experimental support for the preparation and application of two-dimensional materials, nanozymes and sensing devices.

1. Introduction

Black phosphorus, an allotrope of phosphorus, was synthesized by Bridgman (1914) at first more than a century ago. It has attracted a great deal of scientific and technological attention since 2014, when Zhang and co-workers (Li et al., 2014) prepared few-layer BP nanosheets from bulk black phosphorus crystal, and inspired the enthusiasm of researchers in various fields to explore/develop potential application of BP (Batmunkh et al., 2016; Goswami and Gawande, 2015). Now, it has been proved that BP exhibits outstanding properties such as layer dependent band gap (Gusmão et al., 2018a), high carrier mobility (Rudenko et al., 2016), large specific surface area, and excellent ON/OFF ratio (Zhu et al., 2018). However, bare BP can readily convert to oxides (P_xO_y) in the presence of O_2 and/or H_2O and further decompose into acids or salts within minutes or hours (Abate et al., 2018), thus the real success of practical application of BP is seriously challenged due to its low stability. There is thereby an urgent need but it is still a significant challenge to enhance the stability of BP under ambient conditions. Several strategies so far have been developed to overcome the limitations, including capping layer protection (Wan et al., 2015; Kim et al., 2016; Doganov et al., 2015), covalent aryl diazonium functionalization (Ryder et al., 2016), hetero atoms doping (Yang et al., 2016), ligand surface coordination (Zhao et al., 2016) and hybridization with other chemicals (Sun et al., 2014, 2015; Lei et al.,

* Corresponding author. School of Pharmacy, Jiangxi Science & Technology Normal University, Nanchang, 330013, China.
** Corresponding author. Institute of Functional Materials and Agricultural Applied Chemistry, Jiangxi Agricultural University, Nanchang, 330045, China.
E-mail addresses: xujingkun1971@yeah.com, xujingkun@tsinghua.org.cn (J. Xu), wenyangping1980@jxau.edu.cn (Y. Wen).
[1] These authors contributed equally to the article.

https://doi.org/10.1016/j.bios.2019.111716
Received 25 June 2019; Received in revised form 3 September 2019; Accepted 17 September 2019
Available online 20 September 2019
0956-5663/

2017). The recent success in preparation and modification for few-layer BP suspension triggers the applications of BP in electronic sensors, especially in electrochemical chem/bio sensors (Table S1). Previously, we investigated the film-forming properties of BP-PEDOT:PSS composite and its environmental stability (Zhang et al., 2016). Subsequently, we developed a molecular imprinted polymer nanocomposite composed of BP quantum dots and PEDOT nanorods in sensing of vitamin C (Zhang et al., 2018). Then, a stable BP nanosensor with anti-fouling property was fabricated to detect ochratoxin A (Xiang et al., 2018) and a highly stable BP-nafion composite was applied in sensing of clenbuterol (Ge et al., 2018). Cui and cooperators established a high-sensitive sensing platform based on BP-doped helical carbon nanofibers for the determination of carbendazim (Cui et al., 2017). These BP-based electrochemical sensors (Zhang et al., 2016, 2018; Xiang et al., 2018; Ge et al., 2018; Cui et al., 2017; Niu et al., 2018; Ding et al., 2018; Cai et al., 2019) are capable of detecting analytes and have good anti-fouling capability, but their electrocatalytic activity still remains a problem for sensing sensitivity. Therefore, the discovery of high-sensitive BP-based electrochemical sensors is essential.

Nanozymes, emerging types of enzyme mimics, refer to nanomaterials with intrinsic enzyme-like capability, which can effectively catalyze the conversion of substrate and accord the same mechanism and/or kinetics of natural enzymes (Gao and Yan, 2016). In 2007, Yan's group first proposed that inert Fe_3O_4 magnetic nanoparticles (Gao et al., 2007) have inherent peroxidase-like performance, which quickly aroused widespread attention in nanotechnology and nanomaterials. From that time, about 50 kinds of inorganic/organic nanomaterials have been confirmed to have intrinsic catalytic performance similar to natural enzymes, including vanadium pentoxide nanoparticles (Ganganboina and Doong, 2018), gold nanoparticles (Darabdhara et al., 2019), platinum nanoparticles (Liu et al., 2018), copper oxide nanoparticles (Liu et al., 2019), cerium oxide nanoparticles (Singh and Singh, 2019), graphene oxide (Tian et al., 2018) and carbon nanotubes (Song et al., 2010). These nanozymes have shown great potential in biomimetic sensors, cancer diagnostics and therapy, immunoassay, and environmental engineering. Wei and Wang reviewed nanomaterials with enzyme-like characteristics (nanozymes) for next-generation artificial enzymes again after a lapse of six years (Wei and Wang, 2013; Wu et al., 2019), suggested that nanozymes have become the new star in the field of nanotechnology and hot topics of the new artificial mimic enzymes. Rapid development of preparation and surface modification of nanozymes (Liu and Liu, 2017; Wang et al., 2018a) conversely promote the extensive concern of the nanozymes in academia and business. Meanwhile, nanozymes were further introduced into electrochemical sensors. Xu et al. established a dual nanozyme based on AuPd alloy nanoparticles and graphene quantum dots for electrochemical detection in clinic cancer samples (Xu et al., 2018). Qiu and co-authors designed an amino acid conjugated nanozyme and successfully used in electrochemical detection of three organophosphorus pesticides (Qiu et al., 2019). Wang et al. designed a novel nanozyme based on Fe_3O_4 nanoparticles@thionine-imprinted polydopamine (Wang et al., 2017), which could be used in electrochemical detection of hydrogen peroxide, acetylthiocholine chloride, acetylcholinesterase and choline oxidase.

Herein, inspired by these progress, a simple strategy was established thorough the in-situ reduction of Ag ions (Ag^+) and deposition of Ag nanoparticles (AgNPs) on phosphorene and its nanohybrid with NH_2-MWCNT to enhance environmental stability, life-span, and water-dispersibility of BP nanosheets. NH_2-MWCNT-BP-AgNPs nanocomposite was prepared by ultrasonic-assisted liquid-phase exfoliation with the co-addition of both NH_2-MWCNT and $AgNO_3$ in organic solvent 1-methyl-2-pyrrolidinone (NMP), and subsequently dispersed in carboxymethyl cellulose sodium (CMC) aqueous solution. NH_2-MWCNT-BP-AgNPs nanocomposite with superior electrocatalytic capacity and special enzyme-like characteristics was applied as a novel nanoenzyme sensor for single/simultaneous electrochemical determination of three ATP metabolites (UA, XT and HX) (Scheme S1) by different pulse voltammetry (DPV).

2. Experimental

2.1. Reagents

UA, XT, HX and NMP (99.5% purity, anhydrous) were purchased from Shanghai Aladdin Biochem. Tech. Co. Ltd., China. NH_2-MWCNT (8–15 nm, outer diameter, 50 μm length) and high-quality black phosphorus crystal (BP crystal, 99.99% purity) were obtained from Nanjing XFNANO Mater. Tech. Co. Ltd., China. CMC (n = 500) was attained from TCI (Shanghai) Development Co., Ltd. Other reagents were analytical grade and used as received. 0.1 M phosphate buffer solutions (PBS) were used as the supporting electrolyte and prepared by 0.1 M Na_2HPO_4 and 0.1 M NaH_2PO_4. Deionized water (DI water) was obtained from a Milli-Q water purification system.

2.2. Apparatus

Electrochemical measurements were performed though CHI 660D electrochemical workstation (Chen-Hua, Shanghai, China). A common three-electrode system consisted of a saturated calomel electrode (SCE), a platinum electrode (Pt) and a glass carbon electrode (GCE, 3 mm) was used in electrochemical measurements. The three electrodes served as reference electrode, counter electrode and working electrode, respectively. The surface morphology and composition characterization have been achieved using scanning electron microscopy (SEM, FEI Company, United States), transmission electron microscope (TEM, FEI Company, United States) energy-dispersive X-ray spectroscopy (EDS, EDAX Company, United States) and X-ray photoelectron spectroscopy (XPS, Thermo ESCALAB 250Xi, United States).

2.3. Fabrication of the nanocomposite and modified electrode

Liquid-phase exfoliation is a promising strategy to fabricate various ultra-thin 2D materials due to large-scale, highly efficient and solution process-ability. In this experiment, 5×10^{-3} M $AgNO_3$ (Fig. S1) in 10 mL of NMP were added to a three-necked flask and continuously introduced N_2 into the solution at pre-treatment step, about 5 mg of grinding black phosphorus crystal and 10 mg of NH_2-MWCNT powder were submitted into the NMP solution then. This system was ultrasonically treated at N_2 atmosphere for 6–8 h, and the mixture solution was centrifuged at 12000 rpm for 0.5 h to remove the extra NMP. After that, collected the precipitate and added CMC aqueous solution (0.3 mg/mL) to obtain NH_2-MWCNT-BP-AgNPs aqueous dispersion (Fig. S3).

The GCE was mirror-fine polished with 0.05 μm alumna slurry on chamois leather prior to modification, and ultrasonically washed using nitric acid (1:1), ethanol, and DI water, then 5 μL of NH_2-MWCNT-BP-AgNPs mixture was dropped on the surface of GCE and dried under infrared light.

2.4. Real sample preparation

The bovine serum was collected from the college of animal science and technology in Jiangxi Agricultural University and diluted with 0.1 M PBS (pH = 7.0). Subsequently, an aliquot 5 mL of the test solution was added into the electrolytic cell for simultaneous determination of UA, XT and HX by DPV method using NH_2-MWCNT-BP-AgNPs/GCE.

3. Results and discussion

3.1. Morphological and spectra characterization of NH_2-MWCNT-BP-AgNPs

The morphology and microstructure of ultrasonic-liquid phase

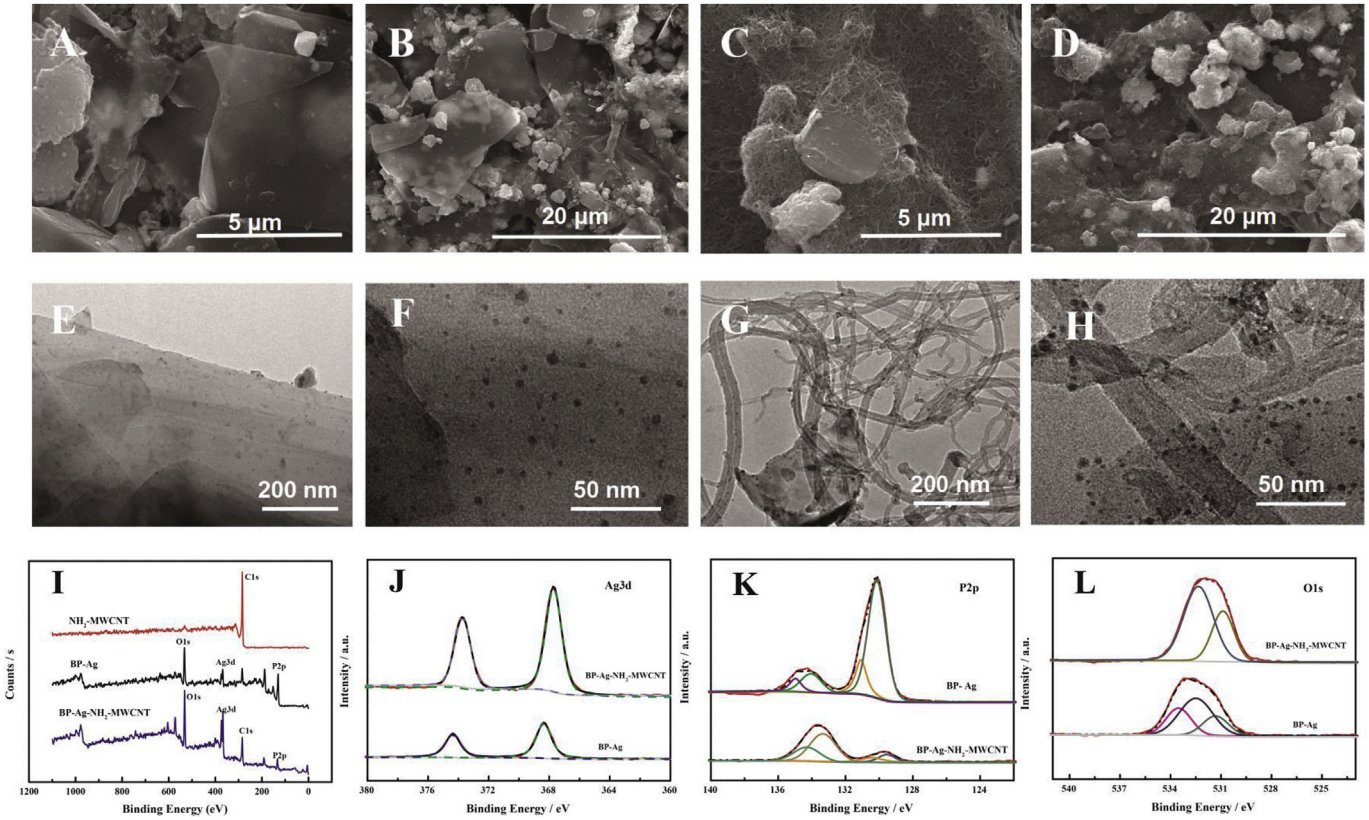

Fig. 1. Typical SEM (A–D) and TEM (E–H) images of BP-AgNPs and NH_2-MWCNT-BP-AgNPs at different scales and corresponding XPS spectra (I–L).

exfoliated BP-AgNPs and NH_2-MWCNT-BP-AgNPs were further characterized by SEM, TEM combined with EDS. Large and ultra-thin BP nanosheets can be readily observed (Fig. 1A) and the nanosheets formed visible wrinkled structure comprising few-layer sheets (Fig. 1B) due to an-isotropic performance of intrinsic black phosphorus (Li et al., 2014; Wood et al., 2014). The special structure supported an ideal condition for anchoring of different small molecules to improve the defects of BP and thus giving potential functionalism to BP nanosheets (Gusmão et al., 2018b). As seen in Fig. 1F, AgNPs were successfully anchored and well-dispersed on the surface of BP nanosheets. Corresponding EDS image (Fig. S2) certificated that the volume of O element was negligible with the presence of AgNPs in BP nanosheets, suggesting that after the redox reaction between BP and Ag^+ (Cho et al., 2017; Wang et al., 2018b), AgNPs anchored on the BP surface and the formation of AgP_xO_y kept the BP from decomposition. The morphology of the NH_2-MWCNT-BP-AgNPs was shown in Fig. 1C, NH_2-MWCNT had successfully covered on the surface of BP nanosheets. When simultaneously introduced Ag^+ and NH_2-MWCNT into the modification process, thin flake-like sheet structure originated from BP and twisted tubular structure originated from NH_2-MWCNT can be clearly observed (Fig. 1G), the few-layered BP nanosheets with large surface area served as a two-dimension substrate for the composition and growth of NH_2-MWCNT.

XPS spectra were also carried out to certificate the surface composition of the BP-AgNPs and NH_2-MWCNT-BP-AgNPs nanohybrid. As shown in Fig. 1I, none of Ag, P and O can be observed in initial NH_2-MWCNT while Ag, P, C, and O were all detected in NH_2-MWCNT-BP-AgNPs. Besides, the high-resolution Ag 3d spectrum of NH_2-MWCNT-BP-AgNPs located at 367.7 eV (Ag $3d_{5/2}$) and 373.7 eV (Ag $3d_{3/2}$) and the slitting of the 3d doublet of Ag was 6.0 eV, which ascribed to metallic silver (Ag^0) and well confirmed the presence and statue of Ag in the nanocomposite. Interestingly, the complex of NH_2-MWCNT-BP-AgNPs was evidenced through the decrease in the binding energy values of 3d doublet when compared to their initial values in BP-AgNPs as 368.4 eV and 374.4 eV, respectively (Fig. 1J). Fitting analysis showed that the P 2p peaks of NH_2-MWCNT-BP-AgNPs could be deconvoluted into four peaks at 129.5, 130.4, 133.3 and 134.3 eV. The peaks at 129.5 and 130.4 eV were relative to P $2p_{3/2}$ and P $2p_{1/2}$ of the P═P bonds, which are typical characteristic of crystalline BP. In addition, the peaks at 133.3 and 134.3 eV were ascribed to P—O—P and O—P—O, which originated from oxygen defects or surface suboxides on the BP surfaces. Moreover, the two changed O1s peaks in both BP-AgNPs and NH_2-MWCNT-BP-AgNPs at binding energy of 530.9 and 532.4 eV were assigned to P═O and P—O—H while the weak oxidation peak at 533.5 eV may rise from P—Ag. (Fig. 1L). These results revealed that the collective introduce of Ag nanoparticles and NH_2-MWCNT will constitute a protective layer that prevented degradation of BP under the condition containing water and consequently leading to excellent stability.

3.2. Water dispersibility, electrochemical characterization and stability

The dispersibility of BP-AgNPs and NH_2-MWCNT-BP-AgNPs in organic solvent and aqueous solution can be seen in Fig. S3, both BP-AgNPs and NH_2-MWCNT-BP-AgNPs showed good dispersibility at first, after being place for a while, the composites in NMP solution precipitated but kept the initial statue in water or CMC solution, demonstrating that BP-AgNPs possessed satisfactory dispersibility in water. What's more, CMC served as an exceeding dispersant and stabilizing agent not only prevented the aggregation but also improved the water dispersibility and stability of NH_2-MWCNT-BP-AgNPs.

To investigate the interface properties of the modified electrode, electrochemical impedance spectroscopy (EIS) was carried out in 5 mM $[Fe(CN)_6]^{3-/4-}$ containing 0.1 M KCl. The electron transfer kinetics of $[Fe(CN)_6]^{3-/4-}$ at bare GCE (a), BP-AgNPs/GCE (b), NH_2-MWCNT/GCE (c) and NH_2-MWCNT-BP-AgNPs/GCE (d) were displayed in Fig. 2A. EIS curve usually includes a semicircle part and a linear part,

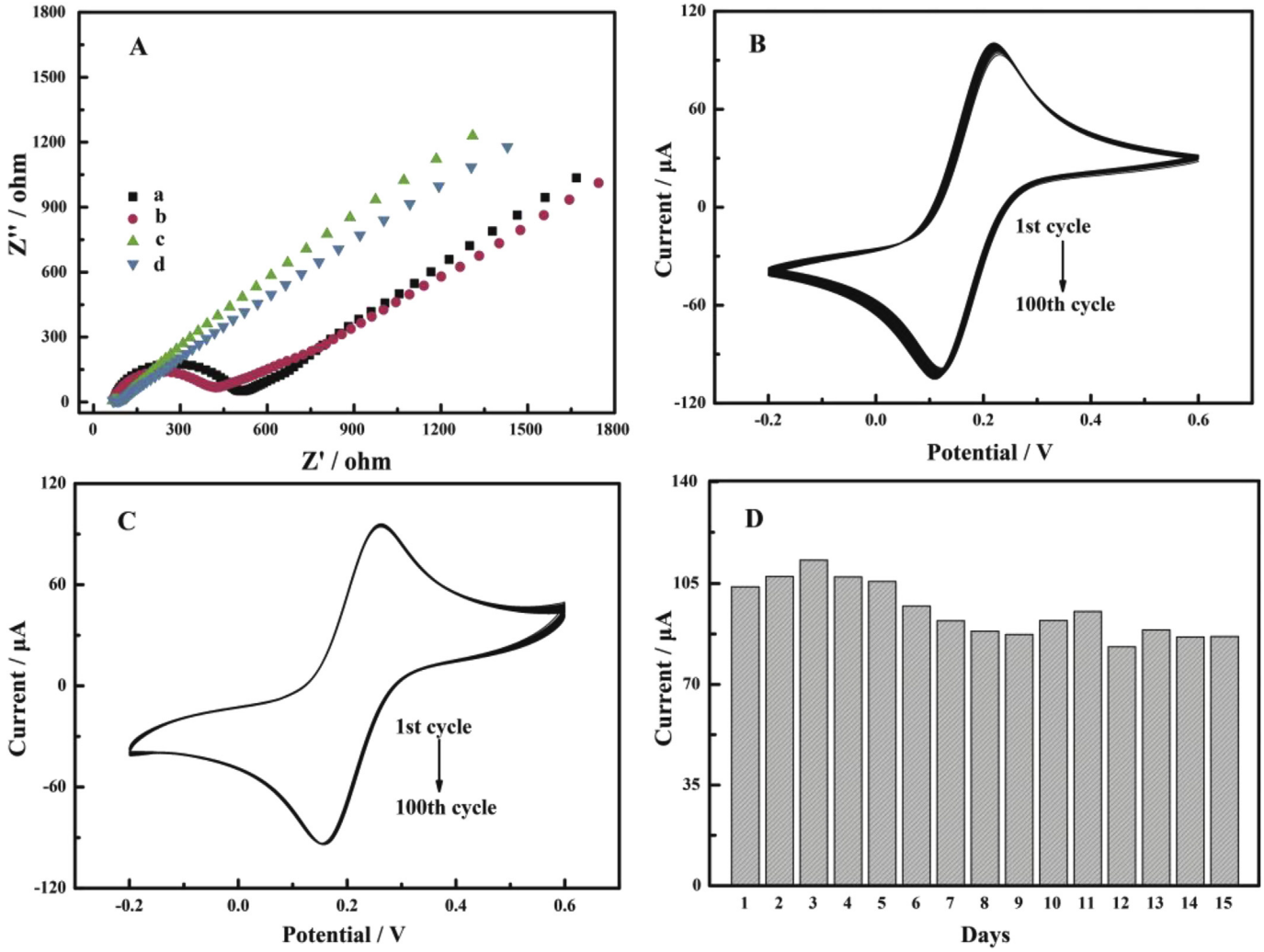

Fig. 2. (A) Nyquist plots of bare GCE (a), BP-AgNPs/GCE (b), NH_2-MWCNT/GCE (c) and NH_2-MWCNT-BP-AgNPs/GCE (d); Cathodic scan 100 CVs of (B) BP-AgNPs and (C) NH_2-MWCNT-BP-AgNPs at 50 mV s^{-1} within the potential window. (D) The oxidation peak currents of NH_2-MWCNT-BP-AgNPs/GCE in 15 days. All the tests were done in 5 mM $[Fe(CN)_6]^{3-/4-}$ containing 0.1 M KCl.

the former at high frequencies relates to the electron transfer limited process, in conformity to the charge transfer resistance (R_{ct}), while the latter at low frequencies relates to the diffusion process. The R_{ct} could be estimated by the diameter of the semicircle in Nyquist plots of EIS and ordered as below: GCE > BP-AgNPs > NH_2-MWCNT ≈ NH_2-MWCNT-BP-AgNPs, which demonstrated that NH_2-MWCNT-BP-AgNPs was smoothly immobilized on the surface of GCE and had better electrochemical property. In terms of the rate-limiting step (diffusion or adsorption) and heterogeneous electron-transfer rates in 5 mM $[Fe(CN)_6]^{3-/4-}$ containing 0.1 M KCl could be seen in Fig. S4, both peaks kept practically unchanged shapes from 10 to 500 mV s^{-1}. The anodic and cathodic currents of the faradaic process increased linearly with square roots of scan rate ($v^{1/2}$) and the plots of $I_{p,a}$ *vs* $v^{1/2}$, $I_{p,c}$ *vs* $v^{1/2}$ were found to linear with slopes of 1.030 (R^2 = 0.982) and −0.885 (R^2 = 0.988), respectively, which revealed a diffusion-controlled process.

Besides, the cycle stability of BP-AgNPs and NH_2-MWCNT-BP-AgNPs were compared by performing successive CV for 100 cycles in 5 mM $[Fe(CN)_6]^{3-/4-}$ containing 0.1 M KCl. It's obvious to see the significantly changing CVs of BP-AgNPs and almost unchanged CVs of NH_2-MWCNT-BP-AgNPs during the 100 cycles tests (Fig. 2B and C). For BP-AgNPs, the relative standard deviation (RSD) values of $I_{p,a}$ and $I_{p,c}$ were 1.36% and 1.22%, while the RSD values of $I_{p,a}$ and $I_{p,c}$ belonged to NH_2-MWCNT-BP-AgNPs were 0.37% and 0.35%, respectively. The negligible variation suggested the superior cycle stability of NH_2-MWCNT-BP-AgNPs, which is consistent with the observation from the overlap figures (Fig. S5) about the first cycle and the 100th cycle of BP-AgNPs and NH_2-MWCNT-BP-AgNPs. To investigate the long-term stability of NH_2-MWCNT-BP-AgNPs nanocomposite in ambient environment, the modified electrode was stored at 4 °C and tested every day, while subsequent oxidation peak current analysis yielded more than 90% of their initial values, indicated that the as-prepared sensors had good storage stability and did not undergo surface fouling. All these results suggested that NH_2-MWCNT-BP-AgNPs nanocomposite had better electrochemical cycle stability in aqueous solution containing oxygen and showed long-term stability.

3.3. Electrochemical behavior of UA, XT and HX

The sensing performance of bare GCE (a), BP-AgNPs/GCE (b), NH_2-MWCNT/GCE (c), and NH_2-MWCNT-BP-AgNPs/GCE (d) in 0.1 M PBS (pH = 7.0) by DPV (Fig. 3). At bare GCE, only a broad peak at 0.72 V can be seen while the oxidation peaks corresponding to UA and HX cannot be identified clearly. Thus, it is almost impossible to use bare GCE for simultaneous determination of these analytes even in high concentration (curve a). When modified with BP-AgNPs, HX can be identified and the $E_{p,a}$ of UA and XT both shift negatively (curve b). In addition, outstanding signal amplification capacity for UA, XT, HX can

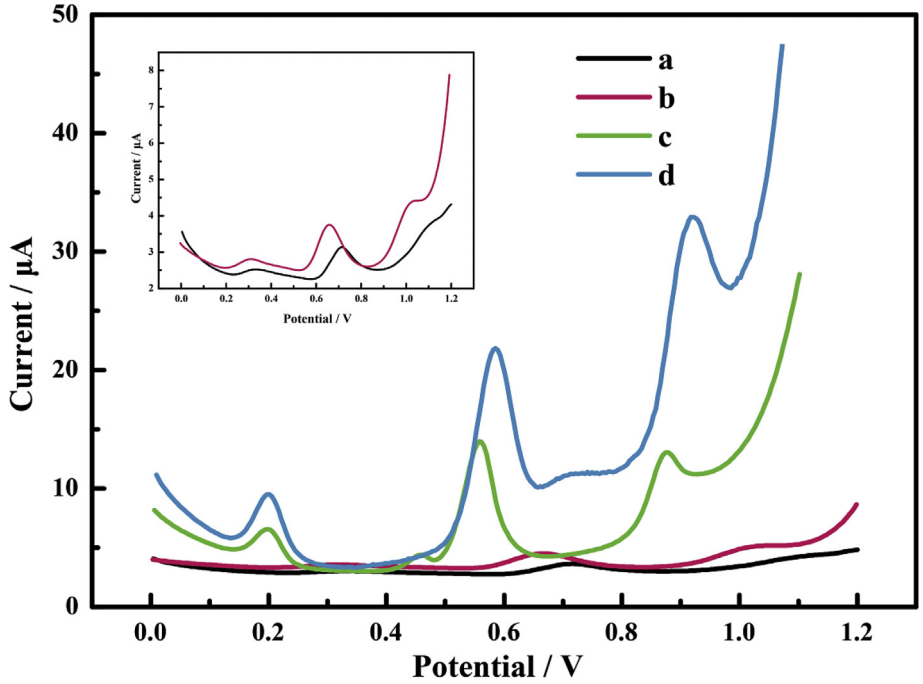

Fig. 3. DPVs of UA (60 μM), XT (60 μM) and HX (60 μM) at bare GCE (a), BP-AgNPs/GCE (b), NH_2-MWCNT/GCE (c) and NH_2-MWCNT-BP-AgNPs/GCE (d) in 0.1 M PBS (pH = 7.0).

be observed at NH_2-MWCNT/GCE (curve c) and NH_2-MWCNT-BP-AgNPs/GCE (curve d), both overpotential at the modified electrodes reduced, which is consistent with the performance of nanozyme (Nasir et al., 2017). Compared with NH_2-MWCNT/GCE, the peak-to-peak spacing of UA-XT, XT-HX and UA-HX were 0.39 V, 0.34 V and 0.72 V, indicated that it could be used in selective and simultaneous determination of the three analytes in their mixture.

3.4. Parametric optimization of NH_2-MWCNT-BP-AgNPs nanosensor

The effects of scan rate (v) on the peak currents ($I_{p,a}$) were investigated to study the kinetics of the electrode reaction. Fig. S6 showed the CVs of UA (60 μM), XT (60 μM) and HX (60 μM) at NH_2-MWCNT-BP-AgNPs/GCE in 0.1 M PBS (pH = 7.0) with the scan rates from 10 to 100 mV s^{-1}. In pace with the increase of scan rate, the oxidation peak current increased obviously and the relevant potential shifted towards a more positive potential as well (Fig. S6A). Apart from this, three bending curves of v-$I_{p,a}$ that belonged to UA, XT, and HX in Fig. S6B and corresponding linear curves between $v^{1/2}$-$I_{p,a}$ in Fig. S6C revealed that there was a diffusion-controlled process for the three analytes on the electrode (Zhang et al., 2015). Besides, the linear relationship between $E_{p,a}$ and ln$v$ of UA, XT and HX could be expressed as: $E_{p,a}$ = 0.011 ln$v$ + 0.260 (R^2 = 0.951), $E_{p,a}$ = 0.022 ln$v$ + 0.260 (R^2 = 0.994), $E_{p,a}$ = 0.024 lnv + 0.905, (R^2 = 0.993), respectively (Fig. S6D), and $E_{p,a}$ could be calculated from the equation of Laviron theory (Laviron, 1979):

$$Ep,\ a = E^0 + \left(\frac{RT}{\alpha nF}\right)\ln\left(\frac{RTk^0}{\alpha nF}\right) + \left(\frac{RT}{\alpha nF}\right)\ln v$$

where $E_{p,a}$ is the peak current potential (V), α is the transfer coefficient, k^0 is the rate constant of the reaction, v is the scan rate, E^0 is the formal standard potential, n is the electron-transfer number, R, T, and F are constant and have their usual meanings (R = 8.314 J mol^{-1} K^{-1}, T = 298 K, and F = 96,485 C mol^{-1}). So the value of αn can be calculated from the slope of $E_{p,a}$-ln$v$, which were 2.33, 1.16, 1.06 and corresponding to UA, XT, and HX. According to the Tafel plot (Fig. S7, Fig. S8), α were evaluated as 0.60, 0.56 and 0.58. Thus, the electron-transfer numbers during the whole process were 4, 2, 2 for UA, XT and HX, which was accord with the previous reports (Struck and Elving, 1965; Dryhurst, 1972).

3.5. Oxidase -like characteristic of NH_2-MWCNT-BP-AgNPs for UA, XT, and HX

DPV method was used to examine the determination of UA, XT, and HX using NH_2-MWCNT-BP-AgNPs modified electrode. With the concentrations of the objects increased, the oxidation peak current responses showed a linear increasing tendency at first and then displayed a gradual deviation from linearity. Moreover, the reciprocal of peak response currents was proportional to the reciprocal of analyte concentrations, suggesting that NH_2-MWCNT-BP-AgNPs has the oxidase-like characteristic (nanozyme) for the electrocatalytic oxidation of UA, XT, and HX.

The apparent Michaelis-Menten constant K_m is a characteristic of biological enzymes, which depicts the enzyme-substrate kinetics of electrochemical enzyme sensors (Liu et al., 2011; Wen et al., 2012) K_m was calculated from the Lineweaver-Burk equation as follows:

$$\frac{1}{I} = \frac{K_m}{I_{\max}}\frac{1}{C} + \frac{1}{I_{\max}}$$

where I is the response current, C is the concentration of the analyte, and I_{max} is the apparent maximum response current. From the curve of Lineweaver-Burk graphs obtained by obtained by $1/I$ versus $1/C$ plots, K_m and I_{max} was estimated.

Take UA as an example, the peak oxidation current increased along with the increase of the concentration of UA from 0.1 to 800 μM (Fig. 4A), while the increments become less and gradually trend to be gentle (inset in Fig. 4B). Then the graphs of was plotted (Fig. 4B), values of K_m and I_{max} of NH_2-MWCNT-BP-AgNPs for UA were estimated as 522.14 μM and 45.45 μA. Similarly, from 0.5 to 680 μM of XT, values of K_m and I_{max} of NH_2-MWCNT-BP-AgNPs were 1160.125 μM and 125 μA (Fig. 4D) while values of K_m and I_{max} of NH_2-MWCNT-BP-AgNPs were for HX were 28.39 μM and 4.74 μA (Fig. 4F) from 1 to 300 μM. The I_{max} is a measure of enzymatic affinity for its substrates, which is inversely proportional to enzymatic affinity for its substrates, indicating that the

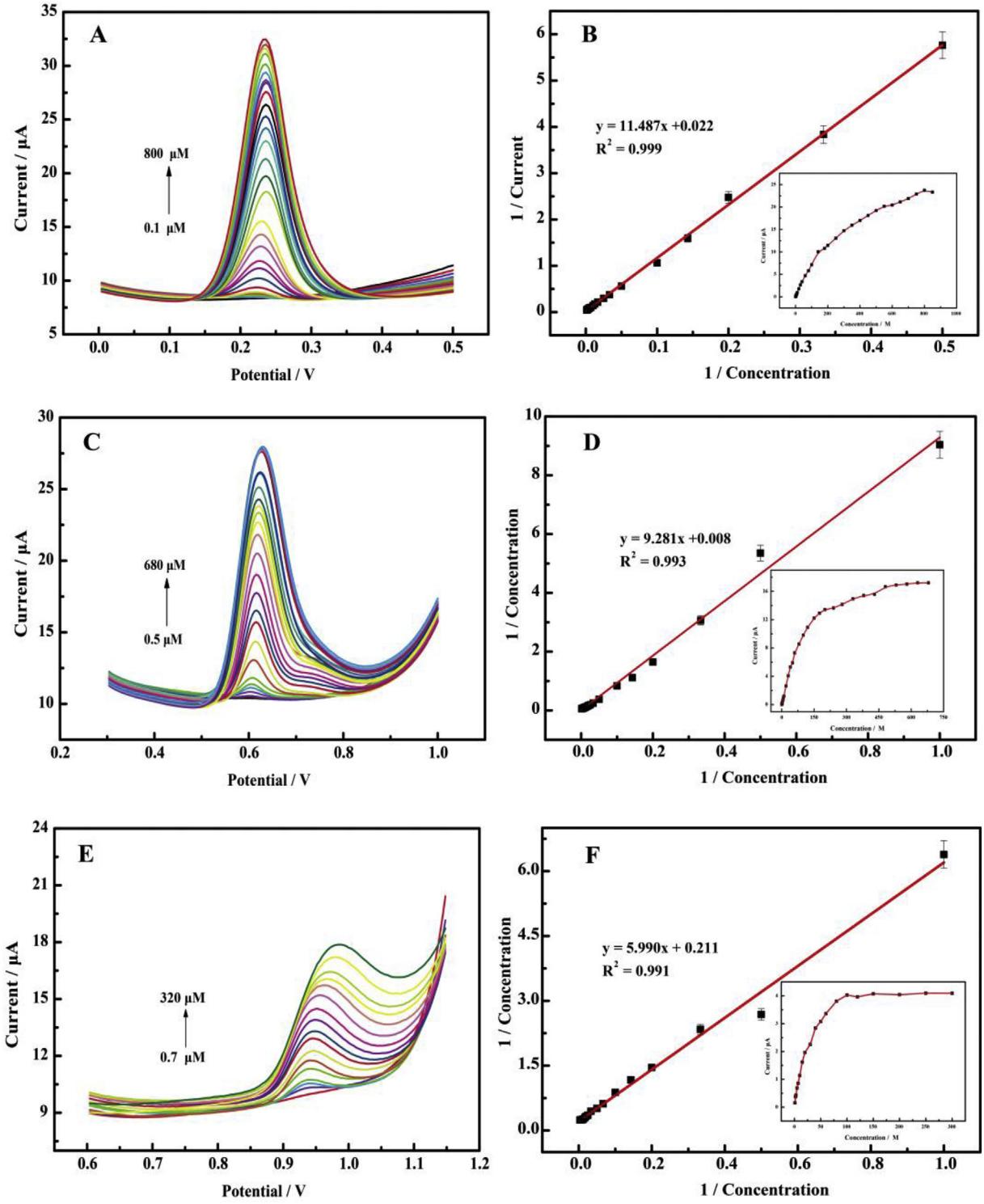

Fig. 4. DPVs of different concentration levels (A) UA (0.1–800 μM), (C) XT (0.5–680 μM), and (E) HX (0.7–320 μM) at NH_2-MWCNT-BP-AgNPs/GCE in 0.1 M PBS (pH = 7.0). Scatchard plots of (B) UA (2–800 μM), (D) XT (1–680 μM) and (F) HX (1–320 μM), respectively. Insets: relationships between $I_{p,a}$ and various concentrations of UA, XT and HX.

effectiveness of this approach in creating high affinity synthetic cavities with binding sites for target molecules due to the interaction between NH_2-MWCNT-BP-AgNPs and analyte.

3.6. NH_2-MWCNT-BP-AgNPs nanozyme for simultaneous sensing of UA, XT and HX

The determination of three analytes was performed in a range from 0 to 1.4 V in 0.1 M PBS (pH = 7.0), when the concentration of one molecular increased and kept the other two subjects unchanged. As shown in Fig. 5A, while maintaining the concentration of XT and HX steadily as 30 and 40 μM respectively, the oxidation peak current of UA increased with the increase of its concentration from 0.3 to 500 μM. No obvious interference can be found for the determination of UA with the coexisting of other two analytes. Similarly, the trend of both XT from 0.3 to 500 μM in the presence of 30 μM UA and 40 μM HX, and HX from

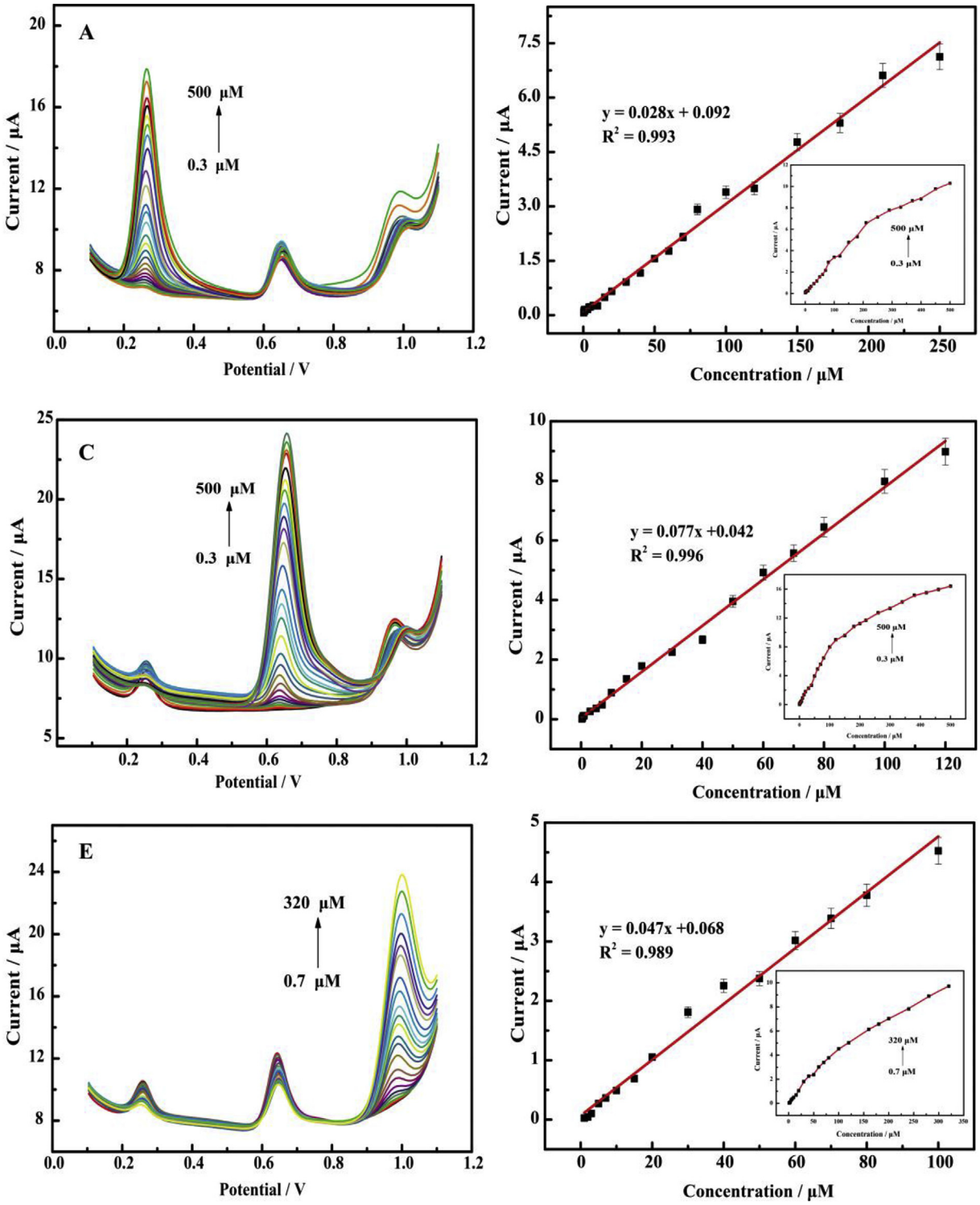

Fig. 5. DPVs obtained for various concentrations of (A) UA (0.3–500 μM) in the presence of 30 μM XT and 40 μM HX, (B) XT (0.5–500 μM) in the presence of 30 μM UA and 40 μM HX and (C) HX (0.7–320 μM) in the presence of 40 μM UA and 40 μM XT at NH_2-MWCNT-BP-AgNPs/GCE in 0.1 M PBS (pH = 7.0). Fig. 5D–F shows the $I_{p,a}$ against the concentration of UA (0.3–250 μM), XT (0.3–120 μM) and HX (0.7–320 μM), respectively. Insets: relationships between $I_{p,a}$ and various concentrations of UA, XT and HX.

0.7 to 320 μM in the presence of 40 μM UA and 40 μM XT are same as UA. The LOD of UA, XT and HX were estimated to be 0.052, 0.021, and 0.025 μM (S/N = 3), and the regression equations have been deduced as: $I_{p,a}$ = 0.028C + 0.092 (R^2 = 0.993) for UA from 0.3 to 250 μM (Fig. 5B), $I_{p,a}$ = 0.077C + 0.042 (R^2 = 0.996) for XT from 0.3 to 120 μM (Fig. 5D) and $I_{p,a}$ = 0.047C + 0.068 (R^2 = 0.990) from 1 to 100 μM (Fig. 5F), respectively, and the sensitivity was assessed by the slope of calibration plot, their sensitivities were 0.028 μA μM^{-1} for UA, 0.077 μA μM^{-1} for XT, and 0.047 μA μM^{-1} for HX. What's more, electrochemical sensors for simultaneous detection of UA, XT and HX were compared between LOD, linear range and sensitivity (Table S2). Accord with Lineweaver-Burk equation and process biomattic enzyme characteristics, it's clearly that NH_2-MWCNT-BP-AgNPs can be used as a novel nanozyme to detect UA, XT and HX.

Table 1
Determination of UA, XT, and HX in bovine serum sample using NH_2-MWCNT-BP-AgNPs nanoenzyme.

	Added (μM)			Found (μM)			Recovery (%)		
	UA	XT	HX	UA	XT	HX	UA	XT	HX
Sample 1	10	10	10	9.83	10.97	9.34	98.3	109.7	93.4
Sample 2	20	20	20	18.18	18.48	21.71	90.9	92.4	108.5

The DPV responses of the three species were recorded by simultaneously changing concentrations of UA, XT and HX in the mixture (Fig. S10A). In concentration ranges of 1–150 μM each at NH_2-MWCNT-BP-AgNPs/GCE in 0.1 M PBS (pH = 7.0), plots of anode peak currents ($I_{p,a}$) and concentrations of the corresponding substance (Fig. S10B) showed similar tendency to that in single determination process, indicating the enzyme-like characteristic (nanozyme) of NH_2-MWCNT-BP-AgNPs for UA, XT, and HX. The values of K_m and I_{max} were 247.87 μM and 33.22 μA for UA (Fig. S10C), 96.25 μM and 31.25 μA for XT and 63.28 μM and 13.69 μA for HX.

3.7. Repeatability and reproducibility

The repeatability of the as-prepared nanozyme sensor was carried out by measuring the peak current response of the modified electrode in the mixed solution containing 20 μM UA, 40 μM XT and 60 μM HX in 5 mL PBS (pH = 7.0). RSD values for anodic peak currents of three substances in 25 successive measurements were 2.72%, 2.69% and 2.24%, respectively (Fig. S11A). Similarly, the reproducibility was investigated by taking seven modified electrodes independently in the mixture containing 60 μM UA, XT and HX, the results yielded RSD values of 2.03%, 1.22% and 2.31% for UA, XT and HX, respectively (Fig. S11B).

3.8. Real sample analysis

Additionally, the practical application of the prepared NH_2-MWCNT-BP-AgNPs nanozyme for simultaneous determination of UA, XT and HX was performed in the samples of bovine serum by utilizing the standard addition method. The three analytes of UA, XT and HX were simultaneously detected using DPV method and the recoveries obtained from spiked samples were between 90.9% and 109.7% (Table 1), which suggested that the proposed method can be utilized in determination of UA, XT and HX in real samples valid with acceptable results.

4. Conclusion

Here, by using Ag^+ and NH_2-MWCNT as the modifiers, high environmental stable and water-processable NH_2-MWCNT-BP-AgNPs nanocomposite was fabricated, which was then characterized using SEM, TEM, EDS and XPS and further applied in single and simultaneous determination of UA, XT and HX through electrochemical method. The NH_2-MWCNT-BP-AgNPs with high conductivity and electrocatalytic capacity not only solved the common and urgent problems of BP nanosheets but also displayed enzyme-like kinetics and characteristics as natural enzymes. Remarkable increase of oxidation peak currents and negative-shift potentials at NH_2-MWCNT-BP-AgNPs/GCE clearly demonstrated that the nanocomposite could be used as an effective additive to promote the kinetics of UA, XT and HX in the electrochemical process. Moreover, the NH_2-MWCNT-BP-AgNPs modified electrode showed exceptional cycle stability, reproducibility and repeatability in the electrochemical process, combined with the acceptable recoveries of real samples, the nanocomposite provided a promising alternative in routine sensing applications of UA, XT and HX.

CRediT authorship contribution statement

Ting Xue: Conceptualization, Funding acquisition, Formal analysis, Writing - original draft, Data curation, Investigation, Writing - review & editing. **Yingying Sheng:** Conceptualization, Funding acquisition, Formal analysis, Data curation, Resources, Writing - original draft. **Jingkun Xu:** Writing - original draft, Funding acquisition, Project administration, Supervision, Writing - review & editing. **Yingying Li:** Formal analysis, Investigation, Methodology. **Xinyu Lu:** Funding acquisition, Investigation, Methodology, Validation. **Yifu Zhu:** Funding acquisition, Writing - original draft, Methodology, Software, Validation, Visualization, Writing - review & editing. **Xuemin Duan:** Writing - original draft, Funding acquisition, Project administration, Supervision. **Yangping Wen:** Conceptualization, Writing - original draft, Funding acquisition, Investigation, Project administration, Resources, Supervision, Writing - original draft, Writing - review & editing.

Declaration of competing interest

The authors declare that they have no known competing financial interests or personal relationships that could have appeared to influence the work reported in this paper.

Acknowledgement

The work was supported by the National Natural Science Foundation of China (51863009, 51662014, 51962007), the Natural Science Foundation of Jiangxi Province (20192ACBL21015), 5511 Science and Technology Innovation Talent Project of Jiangxi Province (20165BCB18016), and Education Department of Jiangxi Province (GJJ160351, GJJ160412).

Appendix A. Supplementary data

Supplementary data to this article can be found online at https://doi.org/10.1016/j.bios.2019.111716.

References

Abate, Y., Akinwande, D., Gamage, S., Wang, H., Snure, M., Poudel, N., 2018. Adv. Mater. 30, 1704749.
Batmunkh, M., Bat-Erdene, M., Shapter, J.G., 2016. Adv. Mater. 28, 8586–8617.
Bridgman, P.W., 1914. J. Am. Chem. Soc. 36, 1344–1363.
Cai, J., Sun, B., Li, W., Gou, X., Gou, Y., Li, D., 2019. J. Electroanal. Chem. 835, 1–9.
Cho, S., Koh, H., Yoo, H., Jung, H., 2017. Chem. Mater. 29, 7197–7205.
Cui, R., Xu, D., Xie, X., Yi, Y., Quan, Y., Zhou, M., 2017. Food Chem. 221, 457–463.
Darabdhara, G., Bordoloi, J., Manna, P., Das, M.R., 2019. Sens. Actuators, B 285, 277–290.
Ding, H., Zhang, L., Tang, Z., Dong, Y., Chu, X., 2018. J. Electroanal. Chem. 824, 161–168.
Doganov, R.A., O'Farrell, E.C.T., Koenig, S.P., Yeo, Y., Zilletti, A., Calvalho, A., 2015. Nat. Commun. 6, 6647.
Dryhurst, G., 1972. J. Electrochem. Soc. 119, 1659–1664.
Ganganboina, A.B., Doong, R., 2018. Sens. Actuators, B 273, 1179–1186.
Gao, L., Yan, X., 2016. Sci. China Life Sci. 59, 400–402.
Gao, L., Zhuang, J., Nie, L., Zhang, J., Zhang, Y., Gu, N., 2007. Nat. Nanotechnol. 2, 577.
Ge, Y., Camarada, M.B., Xu, L., Qu, M., Liang, H., Zhao, E., 2018. Microchim. Acta 185, 566.
Goswami, A., Gawande, M.B., 2015. Front. Chem. Sci. Eng. 1–14.
Gusmão, R., Sofer, Z., Bouša, D., Pumer, M., 2018a. ACS Appl. Energy Mater. 1, 503–509.
Gusmão, R., Sofer, Z., Pumera, M., 2018b. ACS Nano 12, 5666–5673.
Kim, J., Baek, S.K., Kim, K.S., Chang, Y.J., Choi, E.J., 2016. Curr. Appl. Phys. 16, 165–169.
Laviron, E., 1979. J. Electroanal. Chem. Interfacial Electrochem. 101, 19–28.
Lei, W., Liu, G., Zhang, J., Liu, M., 2017. Chem. Soc. Rev. 46, 3492–3509.
Liu, B., Liu, J., 2017. Nano Res. 10, 1125–1148.
Li, L., Yu, Y., Ye, G., Ge, Q., Ou, X., Wu, H., 2014. Nat. Nanotechnol. 9, 372–377.
Liu, M., Wen, Y., Li, D., Yue, R., Xu, J., He, H., 2011. Sens. Actuators, B 159, 277–285.
Liu, J., Meng, L., Fei, Z.F., Dyson, P.J., Zhang, L., 2018. Biosens. Bioelectron. 121, 159–165.
Liu, W., Gan, C., Chang, W., Qileng, A., Lei, H., Liu, Y., 2019. Anal. Chim. Acta 1054, 128–136.
Niu, X., Weng, W., Yin, C., Niu, Y., Li, G., Dong, R., 2018. J. Electroanal. Chem. 811, 78–83.

Nasir, M., Nawaz, M., Latif, U., Yaqub, M., Hayat, A., Rahim, A., 2017. Microchim. Acta 184, 323–342.
Qiu, L., Lv, P., Zhao, C., Feng, X., Fang, G., Liu, J., 2019. Sens. Actuators, B 286, 386–393.
Rudenko, A.N., Brener, S., Katsnelson, M.I., 2016. Phys. Rev. Lett. 116, 246401.
Ryder, C.R., Wood, J.D., Wells, S.A., Yang, Y., Jariwala, D., Marks, T.J., 2016. Nat. Chem. 8, 597.
Singh, R., Singh, S., 2019. Colloids Surf., B 175, 625–635.
Song, Y., Wang, X., Zhao, C., Qu, K., Ren, J., Qu, X., 2010. Chem. Eur J. 16, 3617–3621.
Struck, W.A., Elving, P.J., 1965. Biochem 4, 1343–1353.
Sun, J., Lee, H.W., Pasta, M., Yuan, H.T., Zheng, G.Y., Sun, Y.M., 2015. Nat. Nanotechnol. 10, 980.
Sun, J., Zheng, G., Lee, H.W., Liu, N., Wang, H.T., Yao, H.B., 2014. Nano Lett. 14, 4573–4580.
Tian, L., Qi, J., Qian, K., Oderinde, O., Cai, Y., Yao, C., 2018. Sens. Actuators, B 260, 676–684.
Wan, B., Yang, B., Wang, Y., Zhang, J., Zeng, Z., Liu, Z., 2015. Nanotechnol 26, 435702.
Wang, L., Miao, L., Yang, H., Yu, J., Xie, Y., Xu, L., 2017. Sens. Actuators, B 253, 108–114.
Wang, Q., Wei, H., Zhang, Z., Wang, E., Dong, S., 2018a. TrAC Trends Anal. Chem. (Reference Ed.) 105, 218–224.
Wang, X., Zhou, B., Zhang, Y., Liu, L., Song, J., Hu, R., 2018b. J. Alloy. Comp. 769, 316–324.
Wei, H., Wang, E., 2013. Chem. Soc. Rev. 42, 6060–6093.
Wen, Y., Xu, J., Liu, M., Li, D., Lu, L., Yue, R., He, H., 2012. J. Electroanal. Chem. 674, 71–82.
Wood, J., Wells, S., Jariwala, D., Chen, K., Cho, E., Sangwan, V., 2014. Nano Lett. 14, 6964–6970.
Wu, J., Wang, X., Wang, Q., Lou, Z., Li, S., Zhu, Y., 2019. Chem. Soc. Rev. 48, 1004–1076.
Xiang, Y., Camarada, M.B., Wen, Y., Wu, H., Chen, J., Li, M., 2018. Electrochim. Acta 282, 490–498.
Xu, Q., Yuan, H., Dong, X., Zhang, Y., Asif, M., Dong, Z., 2018. Biosens. Bioelectron. 107, 153–162.
Yang, B., Wan, B., Zhou, Q., Wang, Y., Hu, W., Lv, W., 2016. Adv. Mater. 28, 9408–9415.
Zhang, J., Ding, W., Zhang, Z., Xu, J., Wen, Y., 2016. RSC Adv. 6, 76174–76182.
Zhang, J., Xu, J., Wen, Y., Wang, Z., Zhang, H., Ding, W., 2015. J. Electroanal. Chem. 751, 65–74.
Zhang, Z., Li, Y., Xu, J., Wen, Y., 2018. J. Electroanal. Chem. 814, 153–160.
Zhao, Y., Wang, H., Huang, H., Xiao, Q., Xu, Y., Guo, Z., 2016. Angew. Chem. Int. Ed. 55, 5003–5007.
Zhu, X., Zhang, T., Jiang, D., Duan, H., Sun, Z., Zhang, M., 2018. Nat. Commun. 9, 4177.